IEEE Access
Multidisciplinary : Rapid Review : Open Access Journal

Received 21 September 2022, accepted 6 October 2022, date of publication 17 October 2022, date of current version 21 October 2022.

Digital Object Identifier 10.1109/ACCESS.2022.3215082

RESEARCH ARTICLE

A Novel Practical Decisive Row-Class Entropy-Based Technique for Multilevel Threshold Selection Using Opposition Flow Directional Algorithm

RUTUPARNA PANDA[1], (Member, IEEE), MONORAMA SWAIN[2], (Member, IEEE), MANOJ KUMAR NAIK[3], (Member, IEEE), SANJAY AGRAWAL[1], (Member, IEEE), AND AJITH ABRAHAM[4,5], (Senior Member, IEEE)

[1]Department of Electronics and Telecommunication Engineering, VSS University of Technology, Burla 768018, India
[2]Department of Electronics and Communication Engineering, Silicon Institute of Technology, Bhubaneswar 751024, India
[3]Faculty of Engineering and Technology, Siksha 'O' Anusandhan, Bhubaneswar 751030, India
[4]Machine Intelligence Research Labs, Auburn, WA 98071, USA
[5]Center for Artificial Intelligence, Innopolis University, 420500 Innopolis, Russia

Corresponding author: Rutuparna Panda (r_ppanda@yahoo.co.in)

This work was supported by the Analytical Center for Government of the Russian Federation under Grant 70-2021-00143 dd. 01.11.2021 (IGK000000D730321P5Q0002).

ABSTRACT One of today's inspiring issues is the 2D histogram-based multilevel threshold selection which is used for segmenting images into several regions. The image analysis warrants exploration of multiclass thresholding techniques using various entropy-based objective functions. In this context, the Shannon type of entropic function without inherent decision making capacity has been widely used for threshold selection in the last decade. Furthermore, a 2D histogram was constructed using local average intensity values resulting in loss of some edge information. To address these problems, this study proposes a new methodology using a novel practical decisive row-class entropy (PDRCE) based fitness function for multilevel thresholding. The PDRCE values are computed using the newly constructed 2D histogram-based on normal local variance. Further, an opposition flow directional algorithm (OFDA) is proposed to maximize the fitness function. The performance of the proposed technique is compared with five state-of-the-art 2D histogram-based entropic fitness functions. Moreover, the performance of OFDA is investigated through comparison with other global optimizers namely the genetic algorithm, particle swarm optimization and artificial bee colony. An image segmentation evaluation dataset (BSDS500) is used in this experiment. It is witnessed that the proposal is more efficient than state-of-the-art methods. Our fitness function would be useful for registration, segmentation, fusion, etc.

INDEX TERMS Image processing, multilevel thresholding, entropy, computational intelligence, machine learning.

I. INTRODUCTION

Image segmentation has an important role in several applications. To facilitate a thorough investigation on thresholding based segmentation methods, an effort is made in this paper. Nevertheless, earlier approaches, more or less, are focused on solving the two-class segmentation problems. Subsequently, the multiclass segmentation problem is evolved as a promising area of research. To facilitate a better analysis, the researchers relied on meticulous segmentation of the input images. It is studied from the literature that the multilevel thresholding (MTH) is the easiest way of achieving multiclass

The associate editor coordinating the review of this manuscript and approving it for publication was Muhammad Asif.

segmented outputs. In this context, many methodologies are reported [1], [2], [3], [4], [5], [6], [7], [8], [9], [10], [11], [12]. Most of these methods use the image histogram-based entropy values. Initially, 1D image histogram-based entropy methods were used for this purpose [1]. However, these methods lack the contextual information, which resulted in reduced accuracy. To retain the contextual information, later the idea was extended to 2D image histogram-based entropic functions [2]. The 2D histograms were constructed using the local average versus the grey level pixel intensities. Different objective functions based on 2D histogram were suggested for the purpose. In this study, the reason for inclusion of the references is the domain of interest, i.e., 2D histogram-based MTH methods.

Most of the recent techniques [5], [6], [7], [8], [9], [10], [11], [12] are, more or less, concentrated on the use of the entropic values. The authors in [5] have presented a MTH method based on 2D histogram. They constructed the 2D histogram using the grey-level values of the pixels and the average grey-level values of 3×3 neighbourhood. The diagonal rectangles are used for entropy calculation using Shannon kind of entropic functions. A 2D histogram-based MTH technique was proposed in [6]. These authors [6] also used the similar approach to construct the histogram. They have also used the diagonal regions for computing the Tsallis entropy. Differential evolution (DE) was used for maximization. Fuzzy entropy was used in [7]. The authors in [7] used modified versions of two different evolutionary computation algorithms for optimization. However, the method was similar to the earlier approaches. The authors in [8], [9], and [10] used the 2D Rényi entropy as an objective function for solving the MTH problem. However a 2D histogram is constructed using the lateral inhibition in [10]. Non-extensive entropy based MTH was presented in [11]. The authors in [12] used 2D Masi entropy as the fitness function for solving the MTH problem. Recently, a 2D Kaniadakis entropy-based thresholding technique using 2D histogram is presented in [13]. Lei and Fan [14] suggested the rough entropy based image thresholding. They used the concept of nested optimization for two level image segmentation. The idea of weighted maximum entropy thresholding is discussed in [15]. The method is used for infrared pedestrian segmentation. The authors in [16] reported a generalised Masi entropy based image segmentation algorithm. It is also kept in mind to retain the contextual information by using the 2D histograms. However, there are certain demerits of these existing 2D histogram-based methods. Due to the averaging of the grey-level values in the neighbourhood while construction of the 2D histogram, edge features are not efficiently retained. Moreover, the computations are more, because of the use of the diagonal regions.

In general, different ECs [17], [18], [19], [20], [21] are used to optimize the fitness functions discussed above. Because, the search process becomes exhaustive with increasing number of thresholds. Therefore, there is a necessity to use evolutionary computing (EC) techniques.

The entropic fitness functions used above are not well suited, because the pixel intensities are not uniformly distributed. Moreover, research papers are not seen related to the use of decision making entropy for practical image segmentation applications. To be specific, multilevel threshold selection with inherent decision making is a meaningful research study now. This study encourages us to investigate practical decision making entropy kind of objective functions for multiclass image segmentation, which is a worthwhile idea. This approach is never perceived in the image processing/ computer vision literature.

It may be noted that the earlier methods use Shannon kind of entropy based fitness functions. The logarithmic functions used to compute Shannon type of entropy have their inherent flaws. It is obvious that $-\log p_i = \infty \;, when \quad p_i = 0$ [22]. The notation p_i indicates the probability of occurrence of a particular pixel intensity. As a result, the accuracy value is lessened. In addition, the local averaging adopted while constructing the 2D histogram in the above methods [5], [6], [7], [8], [9], [10], [11], [12] causes loss of the edge information, leading to less accuracy.

This is the reason why the authors are motivated to suggest a novel decisive kind of entropy based objective function, coined as practical decisive row class entropy (PDRCE). Where, we use exponential kind of function with inherent mechanism for practical decision making to compute the PDRCE. Further, the normal local variance in the 2D histogram construction process is incorporated. A new Opposition Flow Directional Algorithm (OFDA) is also suggested for maximizing the PDRCE. The reason for the choice of OFDA is its inherent ability to explore a larger search space. In summary, the contributions are – i) a novel PDRCE based objective function for multilevel thresholding, ii) construction of 2D histogram using normal local variance, iii) a new optimizer called OFDA. This investigation may add new literature to the image segmentation area.

The rest of the sections are organized as follows: Section II describes the materials and methods related to this work. The suggested methodology is presented in Section III. Results and discussions are found in Section IV. Conclusions are drawn in Section V.

II. MATERIALS AND METHODS

The above discussions are very important from an image processing point of view. Thus, we are motivated to investigate a new strategy for multilevel image thresholding using the 2D PDRCE technique.

A. OTSU METHOD

Let us assume that $TH = [th_1, th_2, th_3, \cdots, th_{k-1}]$ comprises many thresholds. In Otsu's scheme, the variance plays an important role in the threshold selection process. It is defined as [1], [2]:

$$\sigma_B^{2^c} = \sum_{i=1}^{k} \sigma_i^{2^c} = \sum_{i=1}^{k} \omega_i^c \left(\mu_i^c - \mu_T^c\right)^2 \tag{1}$$

Here, i is an integer. The probability of occurrence is denoted by ω_i^c, the mean of the i-th class is represented by μ_i^c. For MTH, the ω_i^c values for different i are given below:

$$\omega_0^c(th) = \sum_{i=11}^{th} Ph_i^c, \omega_1^c(th) = \sum_{i=th_1+1} {}_2^{th} Ph_i^c, \cdots, \omega_{k-1}^c(th) = \sum_{i=th_k+1}^{L} Ph_i^c \quad (2)$$

The μ_i^c values for different i are given by:

$$\mu_0^c = \sum_{i=11}^{th} \frac{iPh_i^c}{\omega_0^c(th_1)}, \mu_1^c = \sum_{i=th_1} +1_2^{th} \frac{iPh_i^c}{\omega_1^c(th_2)}, \cdots,$$
$$\mu_{k-1}^c = \sum_{i=th_k+1}^{L} \frac{iPh_i^c}{\omega_{k-1}^c(th_k)} \quad (3)$$

It may be noted that Otsu's between class variance methodology was first proposed for the bi-level thresholding (BTH). Need to mention here that the method is based on the image histogram. Subsequently, the basic idea was extended to the MTH. This method is found popular for the image segmentation.

B. KAPUR'S ENTROPY THRESHOLDING

Another quite popular method (non-parametric) used for the segmentation purposes is Kapur's entropy-based technique. The scheme is found in [5] and [6] for the MTH. Its popularity is mainly for its easiness in the implementation, because it is a non-parametric method. Kapur's-entropy based scheme is mainly dependent on the probability distribution of the pixel intensities. Image histogram is used for computing the entropy values. This is treated as a maximization problem. The fitness function for the BTH using Kapur's entropy is:

$$f_{Kapur} = H_1^c + H_2^c, c = \begin{cases} 1, 2, 3, & for\ RGB \\ 1, & for\ Grayscale \end{cases} \quad (4)$$

The entropies H_1 and H_2 are defined as:

$$H_1^c = \sum_{i=1}^{th} \frac{Ph_i^c}{\omega_0^c} \ln\left(\frac{Ph_i^c}{\omega_0^c}\right), \quad H_2^c = \sum_{i=th+1}^{L} \frac{Ph_i^c}{\omega_1^c} \ln\left(\frac{Ph_i^c}{\omega_1^c}\right) \quad (5)$$

Here, the probability distribution of the grey level is denoted by Ph_i^c. Note that the probability of occurrences are represented by $\omega_0^c(th)$ and $\omega_1^c(th)$, for two distinct classes C_1 and C_2. The idea is also extended to the MTH. In this case, the objective function is expressed by:

$$f_{Kapur}(TH) = \sum_{i=1}^{k} H_i^c, \quad c = \begin{cases} 1, 2, 3, & for\ RGB \\ 1, & for\ Grayscale \end{cases} \quad (6)$$

Here, $TH = [th_1, th_2, \cdots, th_{k-1}]$ contains $(k-1)$ number of thresholds. For MTH, (5) is written by:

$$H_1^c = \sum_{i=11}^{th} \frac{Ph_i^c}{\omega_0^c} \ln\left(\frac{Ph_i^c}{\omega_0^c}\right),$$
$$H_2^c = \sum_{i=th_1+1}^{th_2} \frac{Ph_i^c}{\omega_1^c} \ln\left(\frac{Ph_i^c}{\omega_1^c}\right), \cdots,$$
$$H_k^c = \sum_{i=th_{k-1}+1}^{L-1} \frac{Ph_i^c}{\omega_{k-1}^c} \ln\left(\frac{Ph_i^c}{\omega_{k-1}^c}\right) \quad (7)$$

Precisely, (7) is used to segment the image into multiple classes. More details are found in [5] and [6]

C. THE FLOW DIRECTIONAL ALGORITHM

The flow directional algorithm (FDA) is discussed in [18]. It is inspired by the flow of water into a drainage basin, which simulates the direction of flow to the lowest height outlet points. The flow direction is also influenced by the neighboring flow and its slope, which is based on the D8 cell model (ref Fig. 2 in [18]). Each flow position $Flow\_X$ and its height $Flow_{fitness}(f(flow_X))$ serves as a search agent for α flow, which is initialized in the drainage basin within the boundaries $[ub, lb]$. The new flow positions are estimated in two ways in the FDA. Firstly, it is to assume that a flow generates its β neighbor flow $Neighbor\_X$(ref (3) in [18]) on its route to the drainage basin, and then, updates flow locations $Flow\_newX$(ref (8) in [18]) based on the best neighbor flow. The flow positions are updated $Flow\_newX$(ref (9) in [18]) in a second way by presuming that the present flow encounters any random flow, and changed its path. Finally, the flow's position is updated, if it is better than the old flow, which is expressed as:

$$Flow_{X(i)} = \begin{cases} Flow_{newX(i)} & f\left(Flow_{newX(i)}\right) < f\left(Flow_{X(i)}\right) \\ Flow_{X(i)} & Otherwise \end{cases}$$
$$\forall i \in [1, \alpha] \quad (8)$$

where $f(Flow\_newX(i))$ is the height of $Flow\_newX(i)$. The flow position is updated iteratively until it approaches the optimal solution or maximum iteration Max_Iter. The FDA demonstrated outstanding performances on the benchmark functions. It has also shown better results for the real-world engineering design problems. More information regarding the FDA is found in [18].

III. PROPOSED METHODOLOGY

This section highlights a new model for the multilevel thresholding of images.

A. PROPOSED OBJECTIVE FUNCTION FOR MULTILEVEL THRESHOLDING

Here, we present the PDRCE based threshold selection method for multiclass image segmentation. Fig. 1 displays the block diagram of the PDRCE scheme. The PDRCE values are calculated along the row using the two dimensional histogram of an image. The normal local variance is used for the construction of the two dimensional histogram. Need to mention that the fitness function values are linked to the threshold selection. Therefore, an optimizer is used for obtaining the optimal threshold.

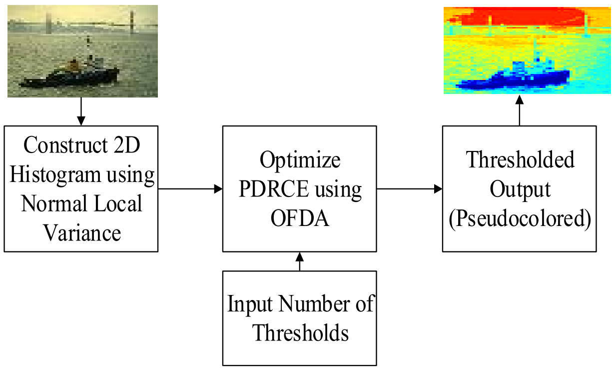

FIGURE 1. Block diagram of the suggested methodology.

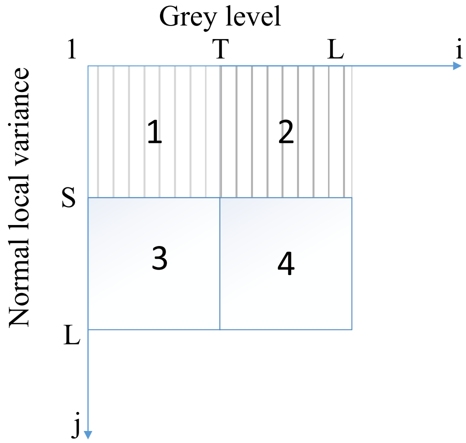

FIGURE 2. Histogram in 2D for single threshold.

Let the grey image be $I \in \Re^{M \times N}$. Let L represents the intensity levels. Here, $z = \{0, 1, 2, \cdots, L-1\}$ is the intensity value of the pixels.

It is noted that $z(x, y)$ denotes the pixel intensity, where (x,y) are the pixel coordinates. Then, the local average $av(x,y)$ is calculated as:

$$av(x, y) = \left\lfloor \frac{1}{w \times w} \sum_{a=-l}^{l} \sum_{b=-l}^{l} f(x + a, y + b) \right\rfloor \quad (9)$$

where, $l = \left\lfloor \frac{w}{2} \right\rfloor$ and w is the size of the window. Generally, the odd numbers are chosen for w.

In this contribution, an effort is made to consider the difference pixel intensities instead of straight forward consideration of the average pixel intensities, as opposed to most of the prevailing methodologies.

In this work, the local variance $lvar(x, y)$ is computed as:

$$l\,\mathrm{var}(x, y) = (z(x, y) - av(x, y))^2 \quad (10)$$

Proper care is taken to suppress high amplitude peaks, which is normally encountered in differential steps. To avoid such a situation, the local variance is further normalized. Interestingly, normalized local variance is more justified for practical applications.

Hence, the $lvar$ is normalized to:

$$l\mathrm{var}_n(x, y) = \frac{(l\mathrm{var}(x, y) - lvar_{\min}) \times L}{l\mathrm{var}_{\max} - l\mathrm{var}_{\min}} \quad (11)$$

where $l\mathrm{var}_{\max}$ and $l\mathrm{var}_{\min}$ are the maximum and minimum values of $l\mathrm{var}(x, y)$ respectively. Need to mention here that L is 256.

Here, $z(x, y)=i$, $l\mathrm{var}_n(x, y)=j$. In this development, note that occurrence of pair $(i, j) = q_{ij}$.

Further, probability of occurrence of (i,j) is given by:

$$p_{ij} = \frac{q_{ij}}{M \times N} \text{with} 1 \le i, j \le L. \quad (12)$$

Figure 2 displays creation of two dimensional histogram suggested for two level thresholding. Note that (S, T) represents the threshold. The histogram is partitioned into four quadrants. Note that the quadrants one and two contain the directed edges. In Fig. 2, the 1st quadrant contains the background (C_1) information, whereas the 2nd quadrant carries the foreground (C_2) information. In this work, C_1 and C_2 represent two distinct classes.

The probability distribution of (C_1) is expressed below:

$$P_1(C_1) = \sum_{i=1}^{S} \sum_{j=1}^{T} p_{ij} \quad (13)$$

The probability distribution of (C_2) is given by:

$$P_2(C_2) = \sum_{i=1}^{S} \sum_{j=T+1}^{L} p_{ij} \quad (14)$$

The corresponding class probabilities of C_1 and C2 are expressed as:

$$C_1 : \left\{ \frac{p_{ij}}{P_1}, i \in 1, 2, \ldots, S; j \in 1, 2, \ldots, T \right\} \quad \text{and}$$

$$C_2 : \left\{ \frac{p_{ij}}{P_2}, i \in 1, 2, \ldots, S; j \in T+1, T+2, \ldots, L \right\}$$

The proposed PDRCE is expressed as:

$$E_1(S, T) = -\sum_{i=1}^{S} \sum_{j=1}^{T} \left(\frac{p_{ij}}{P_1}\right) \exp\left(1 - \left(\frac{p_{ij}}{P_1}\right)^{\alpha}\right) \quad (15)$$

and

$$E_2(S, T) = -\sum_{i=1}^{S} \sum_{j=T+1}^{L} \left(\frac{p_{ij}}{P_2}\right) \exp\left(1 - \left(\frac{p_{ij}}{P_2}\right)^{\alpha}\right) \quad (16)$$

Utilizing the sum property of PDRCE:

$$E_{Total}(S, T) = E_1(S, T) + E_2(S, T) \quad (17)$$

By maximizing E_{Total}, we get the optimal values.

$$(S_{opt}, T_{opt}) = \arg\max \{E_{Total}(S, T)\} \quad (18)$$

Two dimensional histogram for multilevel threshold selection is constructed using our method and is shown in Fig. 3. Here, we assume 2-thresholds; the histogram is divided into 6 distinct areas. Notably, the first row itself contains the required information. It is noteworthy to mention that the first row also preserves the edge information. Further, the process

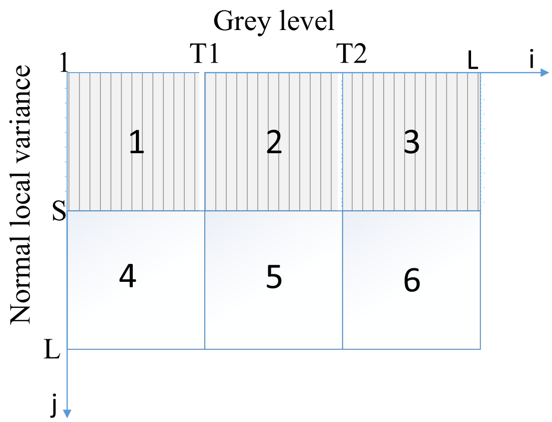

FIGURE 3. Histogram in 2D for two thresholds.

facilitates a reduction in the number of calculations, because one needs to calculate optimum 'S' once only. However, the optimal *T1* and *T2* are calculated twice using two different fitness functions investigated for these thresholds.

Note that the image is partitioned into 'k' number of classes. The probability distributions of different classes $C_1, C_2, \ldots, C_k$ are expressed as:

$$\begin{aligned} P_1(C_1) &= \sum_{i=1}^{S} \sum_{j=1}^{T_1} p_{ij} \\ P_2(C_2) &= \sum_{i=1}^{S} \sum_{j=T_1+1}^{T_2} p_{ij} \\ &\cdots \\ P_k(C_k) &= \sum_{i=1}^{S} \sum_{j=T_{k-1}+1}^{L} p_{ij} \end{aligned} \tag{19}$$

The PDRCEs are defined by:

$$\begin{aligned} E_1(S,T_1) &= -\sum_{i=1}^{S} \sum_{j=1}^{T_1} \left(\frac{p_{ij}}{P_1}\right) \exp\left(1-\left(\frac{p_{ij}}{P_1}\right)^{\alpha}\right) \\ E_2(S,T_2) &= -\sum_{i=1}^{S} \sum_{j=T_1+1}^{T_2} \left(\frac{p_{ij}}{P_2}\right) \exp \\ &\quad \times \left(1-\left(\frac{p_{ij}}{P_2}\right)^{\alpha}\right) \\ &\cdots \\ E_k(S,T_{k-1}) &= -\sum_{i=1}^{S} \sum_{j=T_{k-1}+1}^{L} \left(\frac{p_{ij}}{P_k}\right) \exp \\ &\quad \times \left(1-\left(\frac{p_{ij}}{P_k}\right)^{\alpha}\right) \end{aligned} \tag{20}$$

It is important to remember that 'α' is a tuning parameter.

The total PDRCE is defined as:

$$E_{Total}(ST_1, ST_2, \ldots, ST_{k-1}) = E_1(S,T_1) + E_2(S,T_2) + \ldots + E_k(S,T_{k-1}) \tag{21}$$

Maximizing (21), we get the fitness function:

$$(S_{opt}T_{opt1}, S_{opt}T_{opt2}, \ldots, S_{opt}T_{opt_{k-1}}) = \arg \max_{1\le ST_i \le k-1} \{E_{Total}(ST_1, ST_2, \ldots, ST_{k-1})\} \tag{22}$$

Fig. 4 shows different histograms for Otsu's, Kapur's and our technique. The sample image shown in Fig. 4(a) is taken from the Berkeley Segmentation Dataset (BSDS500) [23]. Its two dimensional histogram deploying Otsu method is displayed in Fig. 4(b). Its 2D histogram utilizing Kapur's method and our technique are shown in Figures 4(c-d). Interestingly, from Figures 4(b-c), it is observed that the diagonals are used to calculate the entropy values. These values are maximized to get the optimum thresholds, in the cases of Otsu and Kapur's schemes. Nonetheless, under a two dimensional setting, the order of the computational complexity is $O(L^{2K})$, with L as the number of grey levels. Hence, the multilevel thresholding techniques, based on the two dimensional histograms, need more computational time. The computational time increases with increased number of K. However, in our case, it is reduced significantly. Need to mention that the proposed technique used a different construction principle using the normalized local variance, as opposed to the existing technologies. Interestingly, it is seen that the first row is only used to calculate the entropy value, which is depicted in Fig. 4(d). In this case, the time complexity is reduced to $O(L^{K+1})$. The more is the number of threshold levels, the more is the gain in the time complexity. Interestingly, the time complexity of the proposed technique is simply 'L' times that of the 1D Otsu scheme. It immediately reminds us that the 1D histogram-based Otsu's scheme needs $O(L^K)$ computations.

The analysis is based on the facts displayed in Fig. 3 for a clarity. It is reiterated that the optimum 'S' is computed once only. Therefore, the proposal is very intriguing and time efficient. Further, the suggested technique may also be very useful for the selection of multiple thresholds.

It is to reiterate here that (22) is the investigated fitness function, which is optimized (maximized) for computing the optimal threshold values. Note that we need (*K-1*) number of thresholds to partition the image into K distinct classes.

Mostly, state-of-the-art methods for MTH use Shannon kind of entropy based objective functions. It is observed that logarithmic functions are used, which have their inherent demerits. For instance, it is observed that $-\log p_i = \infty$ *when* $p_i = 0$. Here, p denotes the probability of occurrence of a particular pixel intensity. Because of this, the logarithmic functions reduce the accuracy value. This is why the authors are inspired to propose a new decisive type of entropy that is more practical. This study could add to the body of knowledge in the field of image segmentation. The proposed practical decisive row class entropy has more advantages than the traditional Shannon kind of entropy utilized earlier. The advantages of our PDRCE are – i) always found non-negative, ii) for a particular p, the entropy value is permanently more compared to Shannon entropy, iii) it is more decisive, hence, more practical, iv) well suited for MTH. Thus, all four good points on the PDRCE encourage the authors for its use in MTH. The novel idea is further explained below.

The key to our success is the use of the practical decisive entropy basis function. It plays an important role for the investigation of novel objective functions derived in (22). The basis function is presented here for a better understanding.

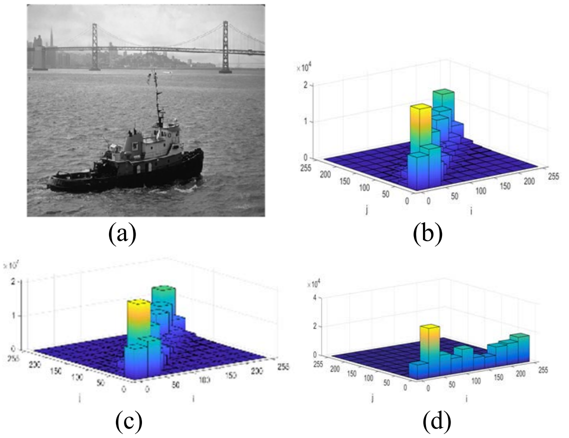

FIGURE 4. Illustration of two dimensional histograms, (a) sample image'#48025', (b) Otsu, (c) Kapur's, (d) Our method.

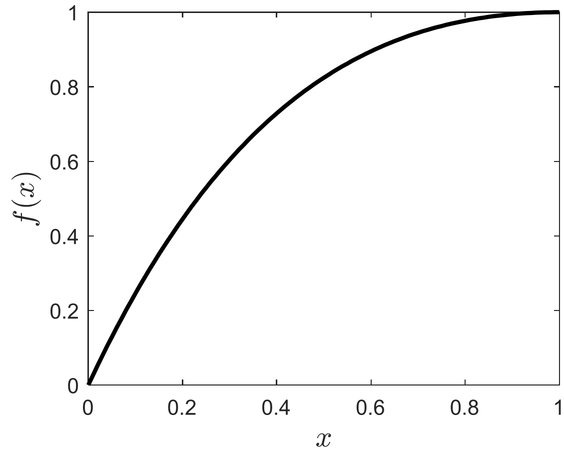

FIGURE 5. A plot of the basis function $f(x)$ with α=1.

To be more specific, the function $f(x) = x\exp(1 - x^{\alpha})$ is used for the development of this methodology, where α is the tuning parameter. The basis function $f(x) = x\exp(1 - x^{\alpha})$ with $\alpha = 1$ is displayed in Fig. 5.

These discussions make the motivation clearer. An appropriate tuning parameter 'α' is used for the decision making. Thus, the derived objective functions are inherently able to handle different situations. The authors of this paper have made an effort to use these functions for the problem on hand.

B. THE PROPOSED OPPOSITION FDA (OFDA)

As discussed earlier, each flow in the FDA updates its solution in the search space based on its random neighbor or some random flow. This may steer the flow to a local optimum solution, which may be a trap. This can be avoided by introducing opposition-based learning (OBL) [19], which aids in the search process in both directions. Let us assume $Flow_{X(i)} = \{Flow\_x(i,1), Flow\_x(i,2), \cdots, Flow\_x(i,d)\}$ be a flow in the d dimensional search space in the range $[LB, UB]$, where $LB = \{lb(1), lb(2), \cdots, lb(d)\}$ and $UB = \{ub(1), ub(2), \cdots, ub(d)\}$. Then, the opposite flow $OFlow\_X(i) = \{OFlow\_x(i,1), OFlow\_x(i,2), \cdots, OFlow\_x(i,d)\}$ is determined as:

$$OFlow\_x(i,j) = ub(j) + lb(j) - Flow\_x(i,j), \forall i \in [1,\alpha] \text{ and } \forall j \in [1,d] \tag{23}$$

Finally, the OFDA's selection-based updating rule is described as follows:

$$Flow_{X(i)} = \begin{cases} OFlow_{X(i)} & f\left(OFlow_{X(i)}\right) < f\left(Flow_{X(i)}\right) \\ Flow_{X(i)} & Otherwise \end{cases} \quad \forall i \in [1,\alpha] \tag{24}$$

where $f(OFlow\_X(i))$ is the height of $OFlow\_X(i)$. The OFDA implementation is illustrated in Fig 6.

IV. RESULTS AND DISCUSSIONS

The results are highlighted in this section. Discussions are also provided for clarity. The parameters for the OFDA are selected based on the guidelines discussed in [18] and [19]. The idea of OFDA is mentioned in the flowchart shown in Fig. 6. Note that the findings are reported after 51 runs of each of the techniques. In this implementation, 40 number of iterations is considered in each run. In this experiment, 300 images from the Berkeley Segmentation Dataset (BSDS500) [23] are used.

The size of the images used is 256×256. These images are converted to the grey scale before the experiment. Our codes are implemented using MATLAB with Core i7 processor having 8GB RAM. Note that $\alpha = 5$ for all the experiments. The results achieved utilizing our technique are marked using boldface letters. In Fig. 7 (a), the sample image (#228076) is displayed. The outputs (segmented version) are pseudo-coloured using MATLAB for effective demonstration. These are also called thresholded images. The suggested methodology is compared with five different state-of-the-art 2D histogram-based entropic methods. Note that, here the results are compared using our implementations for all the methods. In the study, the qualitative and the quantitative results are presented for a fair comparison.

The multiclass outputs are shown for thresholds $TH = 2$, 3, 4 and 5. In Fig. 7, images (b-e) signify the threshold images got deploying the suggested methodology. It is implicit from the figures that more details are noticeable with increasing segmentation classes K.

Interestingly, Fig. 7 depicts that the threshold outputs are very close to the human segmentation images with $K = 6$ and $\alpha = 5$. The reason may be the inherent mechanism of the proposal used to preserve the edge information in a more decisive manner. It is seen that the results with $K = 3$ and 4 exhibits overlapping of various classes. It is noteworthy to mention that significantly improved multiclass segmented outputs are achieved with $K = 6$. The investigated fitness function (PDRCE) is more effective, because it grips the local transitions efficiently. The suggested normal local variance to construct the 2D histogram makes the algorithm more useful for multiclass image segmentation. Because it retains the contextual information efficiently.

More experimental results are added to convince the readers. Fig. 8 displays the results achieved using our methodology. The sample image #296028 from BSDS500 dataset is shown in Fig. 8(a). To illustrate the realistic performances of the proposal, pseudo colours are used. In Fig. 8, images (b-e) epitomize the threshold outputs achieved utilizing the suggested technique. Further, more results are added in Fig. 9. Note that the images in Fig. 9 (b-e) signify the outputs found using the suggested method. A similar observation is obtained from these images.

Table 1 displays a comparison of the PSNR [6] values (computed over 300 images). Note that 'Avg.' indicates the average and 'Std. Dev.' denotes the standard deviation. The PSNR is valuable to compare images taking diverse dynamic ranges. More is the PSNR value, better is the segmentation. A higher value is favorite to claim an improvement in the results, which is obvious for the suggested methodology. To be precise, results using our method exhibit higher values. The possible reason may be its inherent capability to retain all the directional edge information. The contextual information considered during the construction of the 2D histogram helps in boosting the signal info of the output images.

The structured similarity (SSIM) index [6] (computed over 300 images) is shown in Table 2 . The feature similarity (FSIM) [6] index (computed over 300 images) is displayed in Table 3 . It may be noted that all the images are taken from BSDS500 dataset. The higher the values of SSIM and FSIM, the better is the methodology. Hence, always higher values are desired, to achieve a better multilevel thresholding performance. It is seen that (please see Table 2 and Table 3) the average SSIM and FSIM values are best-in-class in the PDRCE. Therefore, better performances are expected, which is implicit. The reason may be the inclusion of the decisive parameter 'α', which improvises the correlation among the pixels. The choice of 'α'is important for the practical. Note that the FSIM is also a well-thought-out metric utilized for assessment. Especially, the gradient magnitude is also more in our method, because it is maximum towards the row as shown in Fig. 3. Hence, Table 3 exhibits higher FSIM values in the proposed case. These SSIM and FSIM values also rise with increasing thresholds (TH).

To support our claim, we present a detail analysis for making the results more convincing for the readers. Fig. 10 displays the graphs for five different functions f_1-f_5. In this figure, $f_1(x) = x\log\left(\frac{1}{x}\right)$; $f_2(x) = x\exp(1 - x^{\alpha=1})$; $f_3(x) = x\exp(1 - x^{\alpha=3})$; $f_4(x) = x\exp(1 - x^{\alpha=5})$; and $f_5(x) = x\exp(1 - x^{\alpha=0.75})$. It may be noted that f_1 is the logarithmic entropic function mostly found in the image processing literature, whereas others (f_2-f_5) are the proposed decisive entropic functions with different values of 'α'. It is wise to iterate that the value of the parameter 'α' plays a crucial role

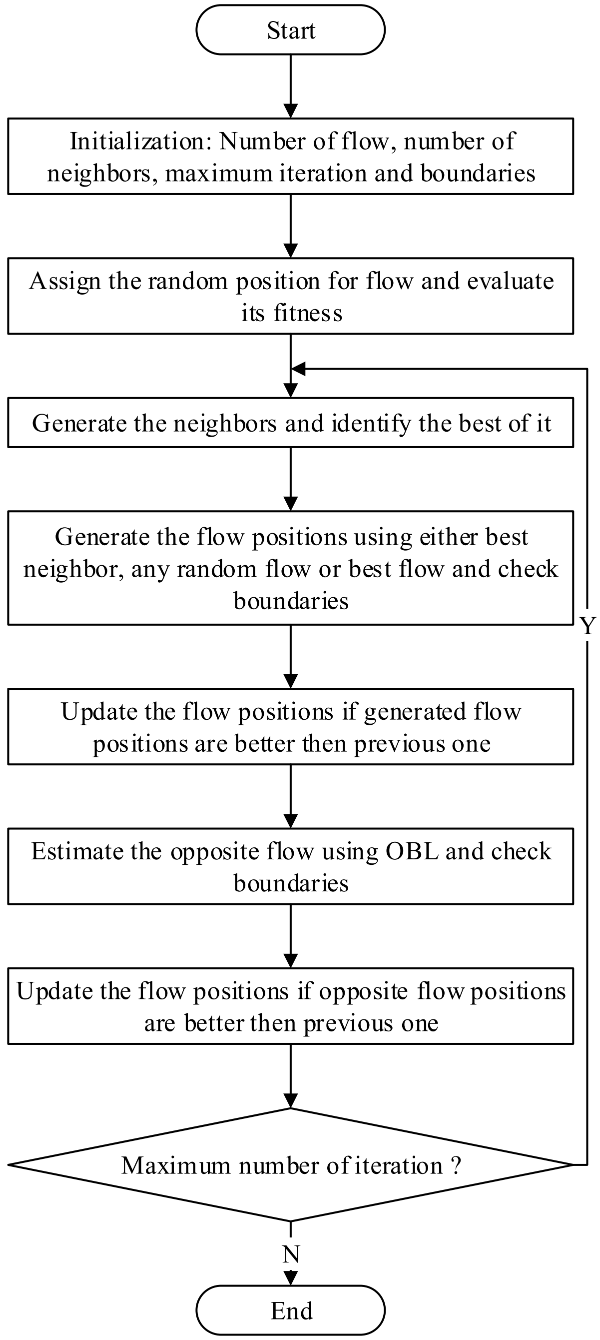

FIGURE 6. Flowchart of the suggested optimizer.

in this development. This makes the method more useful for decision making.

It is noticed that the traditional logarithmic entropy function f_1 has a fixed shape, because it has no inbuilt tuning parameter. On the other hand, we propose an effective basis function that inherently includes the decisive parameter 'α'. Profound differences are observed here by tuning the parameter 'α'. These differences are demonstrated in Fig. 10. It evokes us many interesting ideas. One may easily notice that the value of the suggested entropy is always higher than

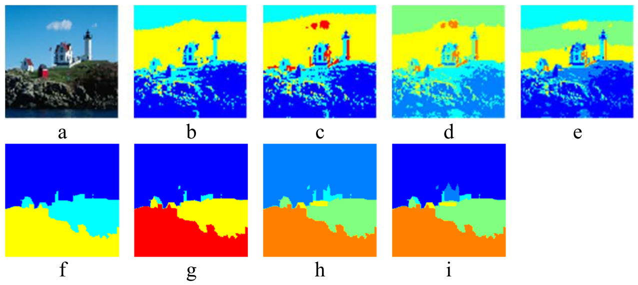

FIGURE 7. Sample image used. (a) Original image #228076 from BSDS500 dataset, (b)-(e) results obtained using PDRCE, (b) 3-level threshold [105,165], (c) 4-level threshold [108,134,171], (d) 5-level threshold [112,137,181,205], (e) 6-level threshold [111,123,167,183,207], (f)-(i) human segmentation outputs. Threshold values used for multilevel thresholding are indicated within the square bracket.

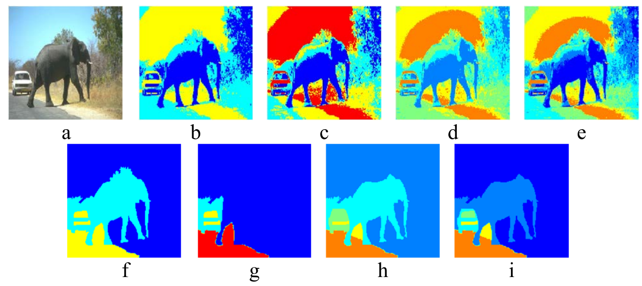

FIGURE 8. Sample image used. (a) Original image #296028 from BSDS500 dataset, (b)-(e) results obtained using PDRCE, (b) 3-level threshold [66,183, (c) 4-level threshold [72,100,185], (d) 5-level threshold [65,94,132,191], (e) 6-level threshold [43,71,108,152,189], (f)-(i) human segmentation outputs. Threshold values used for multilevel thresholding are indicated within the square bracket.

the value of the traditional Shannon type entropy displayed as f_1. This may enrich the image processing literature. The extensive experiments are carried out by varying the values of 'α'. Fourteen different values for 'α' are considered in this exemplar illustration. The outcomes are reported in Table 4. It is found that our method Ranked one with $\alpha = 5$ for the input image #228076. Hence, a value of 5 is chosen for α throughout this work. However, the value may change for other kind of images. This may attract researchers to explore the idea in future applications.

Besides PSNR, SSIM and FSIM, a more detail analysis in terms of the important segmentation indices are provided here. Five indices are explicitly used for comparing the segmentation results. The results are shown in Tables 5-9. The MATLAB codes of these indices together with the benchmark images reported in [22] and [23] are used. The 'ground truth' segmentation images for various scenes are found in [23]. These manually segmented images are often used for the performance evaluation.

It is important to discuss here the importance of the cross correlation (CC) values in the image segmentation [24]. The CC values are displayed in Table 5 . A higher value of CC ensures the efficacy of a method. Our method yields the best values. The use of PDRCE helps us to achieve the best results, which inherently includes the decision making capability. Thus, it is claimed that the suggested technique outperforms the other methodologies reported in Table 5 .

The probability rand index (PRI) is an important segmentation index reported in [24]. The PRI is primarily a measure of the similarity between the ground truth and the output images. Typically, its range lies within [0, 1]. Its value depends on the methodology used. The higher values are desirable for good quality segmentation. The variation of information (VoI) index is also important for evaluating the performance of a segmentation technique [24]. It may be noted that the range of the VoI is $[0, \infty)$. In this case, the lower is the value, the better is the segmentation. The global consistency error (GCE) is yet another important segmentation index used for the performance evaluation. The GCE is reported in [24]. Its range is [0, 1]. It is also widely accepted for the segmentation evaluation. The smaller values are desirable. Similarly,

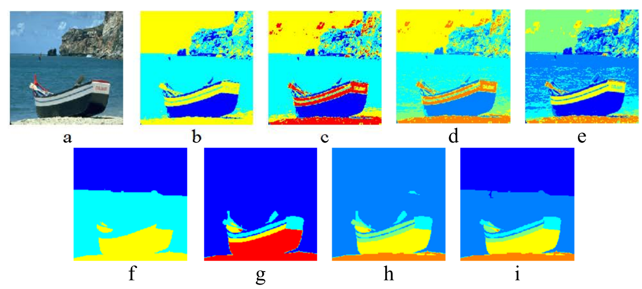

FIGURE 9. Sample image used. (a) Original image #384022 from BSDS500 dataset, (b)-(e) results obtained using PDRCE, (b) 3-level threshold [105,174], (c) 4-level threshold [76,134,179], (d) 5-level threshold [49,103,165,194], (e) 6-level threshold [49,98,134,197,215], (f)-(i) human segmentation outputs. Threshold values used for multilevel thresholding are indicated within the square bracket.

another segmentation index named boundary displacement error (BDE) is also used here to compare the performance of our method. Hence, it is also used for a fair comparison of our method with others. It is noteworthy to mention here that a smaller value of the BDE is desired to claim the superiority of a methodology over others [24]. All these segmentation indices are considered for validation. The results are presented below.

The PRI values are presented in Table 6 . The worthiness of the proposal is implicit. One may see that the suggested methodology ensures improvised results, as opposed to the outputs offered by earlier techniques. It is obvious from Table 6 that these values are more in PDRCE. It is also observed that the values increase with the increasing K, which denotes a worthy multiclass segmentation performance. The BDE values are shown in Table 7 . The best values are also observed in our case. Further, the BDE values become smaller with increasing thresholds, which is implicit in Table 7 . These values are smaller in the proposed case, which is quite desirable.

The GCE values are displayed in Table 8 . In our case, the GCE values are lower than the other techniques; this guarantees the usefulness of the suggested methodology. Even more interesting is that the GCE values are increasing with increasing thresholds (TH). A similar trend is also observed for other cases. The VoI values are shown in Table 9 . The

TABLE 1. Comparison of PSNR values (computed over 300 images from BSDS500 dataset).

Methodology		Number of Thresholds			
		2	3	4	5
PDRCE	Avg.	**67.40**	**69.21**	**70.81**	**71.75**
	Std. Dev.	**1.97**	**2.03**	**2.15**	**2.24**
2D Otsu	Avg.	65.27	66.96	68.20	69.21
	Std. Dev.	2.01	2.07	2.19	2.28
2D Kapur	Avg.	63.63	65.29	66.49	67.48
	Std. Dev.	2.05	2.11	2.24	2.33
2D Kaniadakis	Avg.	61.25	62.89	64.35	65.20
	Std. Dev.	2.11	2.17	2.30	2.40
2D Rényi	Avg.	63.25	64.94	66.44	67.32
	Std. Dev.	2.17	2.23	2.37	2.46
2D Tsallis	Avg.	59.92	61.53	62.95	63.78
	Std. Dev.	2.21	2.27	2.41	2.51

TABLE 2. Comparison of SSIM values (computed over 300 images from BSDS500 dataset).

Methodology		Number of Thresholds			
		2	3	4	5
PDRCE	Avg.	**0.9387**	**0.9669**	**0.9895**	**0.9954**
	Std. Dev.	**0.08**	**0.09**	**0.09**	**0.10**
2D Otsu	Avg.	0.9073	0.9466	0.9661	0.9789
	Std. Dev.	0.08	0.09	0.09	0.10
2D Kapur	Avg.	0.8846	0.9228	0.9418	0.9543
	Std. Dev.	0.09	0.10	0.10	0.11
2D Kaniadakis	Avg.	0.8531	0.8786	0.8992	0.9045
	Std. Dev.	0.09	0.10	0.10	0.11
2D Rényi	Avg.	0.8809	0.9073	0.9285	0.9341
	Std. Dev.	0.09	0.10	0.10	0.12
2D Tsallis	Avg.	0.8345	0.8595	0.8796	0.8849
	Std. Dev.	0.09	0.11	0.11	0.12

TABLE 3. Comparison of FSIM values (computed over 300 images from BSDS500 dataset).

Methodology		Number of Thresholds			
		2	3	4	5
PDRCE	Avg.	**0.9943**	**0.9978**	**0.9976**	**0.9967**
	Std. Dev.	**0.041**	**0.042**	**0.045**	**0.049**
2D Otsu	Avg.	0.9817	0.9907	0.9947	0.9907
	Std. Dev.	0.042	0.043	0.046	0.050
2D Kapur	Avg.	0.9572	0.9660	0.9699	0.9717
	Std. Dev.	0.043	0.044	0.047	0.051
2D Kaniadakis	Avg.	0.9125	0.9157	0.9155	0.9182
	Std. Dev.	0.044	0.045	0.048	0.053
2D Rényi	Avg.	0.9423	0.9455	0.9453	0.9482
	Std. Dev.	0.046	0.047	0.050	0.055
2D Tsallis	Avg.	0.8927	0.8958	0.8956	0.8982
	Std. Dev.	0.047	0.048	0.051	0.056

values in the PDRCE case are found smaller than the other methods. It is worthy to note that the results are compared at a particular threshold level. It is noticed in Table 9 that the values are lower, which is desirable for a better segmentation. An interesting observation is made here. The values of GCE and VoI could have been getting smaller, with an increasing trend of the number of thresholds. However, from Tables 8 and 9, it is seen that these values are increasing. Not

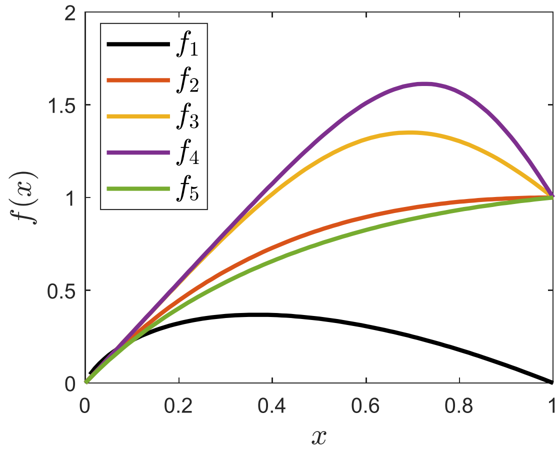

FIGURE 10. A graphical plot showing functions f_1 - f_5.

TABLE 4. Ranking of metrics (average PSNR, average SSIM and average FSIM) with varied parameter α for K=3,4,5 and 6 for the image #228076.

Value of 'α'	Average Rank	Rank
1	11.29	13
2	8.34	9
3	8.03	8
4	4.29	2
5	**2.07**	**1**
6	5.28	4
7	4.75	3
8	6.19	6
9	5.30	5
10	6.17	7
11	9.98	11
12	9.32	10
13	13.26	14
14	11.27	12

TABLE 5. Comparison of CC values (computed over 300 images from BSD300 dataset).

Methodology		Number of Thresholds			
		2	3	4	5
PDRCE	Avg.	**0.9464**	**0.9658**	**0.9794**	**0.9897**
	Std. Dev.	**0.04**	**0.04**	**0.04**	**0.04**
2D Otsu	Avg.	0.9061	0.9494	0.9721	0.9827
	Std. Dev.	0.04	0.04	0.04	0.04
2D Kapur	Avg.	0.8834	0.9257	0.9478	0.9582
	Std. Dev.	0.04	0.04	0.04	0.04
2D Kaniadakis	Avg.	0.8685	0.8863	0.8988	0.9034
	Std. Dev.	0.04	0.04	0.04	0.05
2D Rényi	Avg.	0.8969	0.9152	0.9281	0.9329
	Std. Dev.	0.04	0.05	0.05	0.05
2D Tsallis	Avg.	0.8496	0.8671	0.8792	0.8838
	Std. Dev.	0.05	0.05	0.05	0.05

to be surprised. Perhaps the reason for the trend is the multiclass thresholding methodology itself. The MTH method is different from the traditional segmentation technique. The MTH is, more or less, concentrating on identifying the several objects from the scene.

The statistical t-Test is performed for validating the claim. Table 10 displays the t & p values on the segmentation

TABLE 6. Comparison of PRI values (computed Over 300 images from BSDS500 dataset).

Methodology		Number of Thresholds			
		2	3	4	5
PDRCE	Avg.	**0.5249**	**0.6230**	**0.6577**	**0.6754**
	Std. Dev.	**0.10**	**0.10**	**0.10**	**0.11**
2D Otsu	Avg.	0.4986	0.5919	0.6248	0.6417
	Std. Dev.	0.11	0.11	0.11	0.12
2D Kapur	Avg.	0.4862	0.5771	0.6091	0.6256
	Std. Dev.	0.11	0.12	0.12	0.12
2D Kaniadakis	Avg.	0.4817	0.5718	0.6036	0.6198
	Std. Dev.	0.12	0.12	0.12	0.13
2D Rényi	Avg.	0.4922	0.5841	0.6167	0.6333
	Std. Dev.	0.12	0.13	0.13	0.14
2D Tsallis	Avg.	0.4712	0.5593	0.5905	0.6063
	Std. Dev.	0.14	0.14	0.14	0.15

TABLE 7. Comparison of GCE values (computed over 300 images from BSDS500 dataset).

Methodology		Number of Thresholds			
		2	3	4	5
PDRCE	Avg.	**10.0024**	**8.8988**	**8.5143**	**7.9990**
	Std. Dev.	**0.90**	**0.90**	**0.91**	**0.92**
2D Otsu	Avg.	10.5025	9.3437	8.9400	8.3990
	Std. Dev.	0.95	0.95	0.96	0.97
2D Kapur	Avg.	10.7651	9.5774	9.1635	8.6089
	Std. Dev.	0.96	0.96	0.97	0.98
2D Kaniadakis	Avg.	10.8299	9.6350	9.2186	8.6608
	Std. Dev.	0.97	0.97	0.98	0.99
2D Rényi	Avg.	10.6293	9.4565	9.0479	8.5004
	Std. Dev.	0.97	0.98	0.98	0.99
2D Tsallis	Avg.	11.0303	9.8134	9.3893	8.8211
	Std. Dev.	0.99	0.99	1.00	1.01

TABLE 8. Comparison of BDE values (computed over 300 images from BSDS500 dataset).

Methodology		Number of Thresholds			
		2	3	4	5
PDRCE	Avg.	**0.3496**	**0.5319**	**0.4851**	**0.4566**
	Std. Dev.	**0.11**	**0.11**	**0.12**	**0.13**
2D Otsu	Avg.	0.3671	0.5586	0.5094	0.4795
	Std. Dev.	0.12	0.12	0.13	0.13
2D Kapur	Avg.	0.3763	0.5725	0.5221	0.4914
	Std. Dev.	0.13	0.13	0.14	0.14
2D Kaniadakis	Avg.	0.3784	0.5759	0.5252	0.4944
	Std. Dev.	0.13	0.13	0.14	0.14
2D Rényi	Avg.	0.3715	0.5652	0.5155	0.4852
	Std. Dev.	0.14	0.14	0.15	0.15
2D Tsallis	Avg.	0.3855	0.5866	0.5350	0.5035
	Std. Dev.	0.15	0.15	0.15	0.16

metrics. The t-Test is conducted with a significance level of 0.05 between the PDRCE and the rest methods. Noteworthy differences are observed. The statistical results presented in Table 10 imply that our proposal is significantly different from the other methods.

Here, we add more comparisons between this algorithm and other meta-heuristic algorithms. The performance of the proposed OFDA algorithm is compared with the FDA.

TABLE 9. Comparison of VoI values (computed over 300 images from BSDS500 dataset).

Methodology		Number of Thresholds			
		2	3	4	5
PDRCE	Avg.	**2.6253**	**3.1800**	**3.2109**	**3.2873**
	Std. Dev.	**0.60**	**0.61**	**0.62**	**0.63**
2D Otsu	Avg.	2.7566	3.3390	3.3714	3.4516
	Std. Dev.	0.70	0.72	0.72	0.73
2D Kapur	Avg.	2.8255	3.4224	3.4557	3.5380
	Std. Dev.	0.71	0.74	0.74	0.76
2D Kaniadakis	Avg.	2.8424	3.4431	3.4765	3.5592
	Std. Dev.	0.73	0.73	0.75	0.77
2D Rényi	Avg.	2.7898	3.3793	3.4121	3.4933
	Std. Dev.	0.74	0.74	0.77	0.78
2D Tsallis	Avg.	2.8951	3.5068	3.5408	3.6252
	Std. Dev.	0.79	0.79	0.80	0.81

TABLE 10. Comparison between PDRCE and other methodologies using t-test.

Segmentation Indices		2D Otsu	2D Kapur	2D Kaniadakis	2D Rényi	2D Tsallis
PRI	*t*-value	16.56	16.57	16.39	4.45	16.16
	p-value	0.00	0.00	0.00	0.01	0.00
GCE	*t*-value	-10.57	-10.56	-9.97	-3.03	-10.48
	p-value	0.00	0.00	0.00	0.03	0.00
VOI	*t*-value	-18.13	-18.15	-18.10	-6.59	-17.89
	p-value	0.00	0.00	0.00	0.00	0.00
BDE	*t*-value	-18.65	-18.80	-18.77	-3.87	-17.92
	p-value	0.00	0.00	0.00	0.03	0.00

TABLE 11. Parameters setting.

Optimizer	Parameters	Values
OFDA	size of the population	200
	β	1
FDA	size of the population	200
	β	1
GA	size of the population	200
	crossover probability	0.5
	mutation probability	0.1
PSO	W_{MAX}, W_{MIN}	0.9, 0.1
	size of the swarm	200
	C_1. C_2	2
ABC	size of the population	200
	failure (max_no.)	3
	r(norm), r(power)	2,1

TABLE 12. Comparison of different metrics (computed over 300 images from BSDS500 dataset) using the PDRCE fitness function with other optimizers (threshold level $K = 5$).

Metric	Optimizers				
	OFDA	FDA	GA	PSO	ABC
PRI	**0.6754**	0.6416	0.5944	0.6214	0.6079
GCE	**0.4566**	0.4794	0.5114	0.4931	0.5023
VOI	**3.2873**	3.4517	3.6818	3.5503	3.6160
BDE	**7.9990**	8.3990	8.9589	8.6389	8.7989
CC	**0.9897**	0.9402	0.8709	0.9105	0.8907

In addition, three more popular global optimizers genetic algorithm (GA), particle swarm optimization (PSO), and artificial bee colony (ABC) are also considered for a fair comparison. The parameters setting are displayed in Table 11. All five segmentation indices are considered. The proposed method using FDA, GA, PSO and ABC is also implemented separately. The performance of our method is superior to others. The results are shown in Table 12. It is explicitly clear from the Table 12 that our method performs well while using the OFDA algorithm. The reason may be the enhancement of the search space through opposition learning.

For the sake of completeness, an analysis on the computational complexity is also enlightened here. Nevertheless, 2D Otsu and 2D Kapur schemes offer a time complexity of $O(L^{2K})$, the computation time increases exponentially with increasing K. Whereas, our methodology offers a computation complexity of $O(L^{K+1})$. The reason is that the area used for calculation is limited to one row only (as discussed in Section III). To be precise, the computation time is significantly reduced in our case. Thus, boosting the time efficiency is inhibiting, which may attract the readers.

V. CONCLUSION

In this paper, a novel fitness function coined as PDRCE is proposed for multiclass segmentation. An efficient optimization algorithm named OFDA is suggested. The OFDA's efficacy in achieving the best results are highlighted. The experimental results are shown to justify the use of the PDRCE in the MTH, an important commotion of image processing, a sub-field of the machine intelligence. The multiclass segmentation is created through the maximization of the proposed cost function. The advantages of the PDRCE method are discussed. To figure out – i) decision making is included in the objective function, ii) entropy values are always positive, iii) avoids computation issues even if $p_i = 0$, iv) time complexity is significantly reduced etc. The well-known metrics PSNR, SSIM and FSIM are evaluated and compared with state-of-the-art methodologies. In addition, benchmark segmentation indices are also measured to validate our scheme. A statistical test is performed to ensure the applicability of the proposal in the field of image processing. The suggested PDRCE methodology outperformed earlier techniques. Our technique PDRCE outclassed other state-of-the-art schemes. The reason may be its inherent capabilities to preserve the directional edges in a useful way. In addition, the optimizer OFDA brings in an enhancement of the exploration space, significant abridged calculation difficulty etc. Most importantly, the information is contained in the first row only, yielding reduced computation complexity. Further, Tables 1-9 demonstrate that the performance of our methodology is better compared to state-of-the-art technology. The limitations of the method are – over segmentation may occur when the number of threshold levels are very high. This may be due to the inherent characteristics of the images or limitations of our methodology. The choice of α value is crucial, which may be determined experimentally.

The idea of the PDRCE may be extended to 3D form. The OFDA may be redesigned incorporating the crossover-mutation, chaos, and learning etc. The strategy would be used for the MTH of various medical images. The research idea may also be extended to the segmentation of color images.

REFERENCES

[1] H. Gao, W. Xu, Y. Tang, and J. Sun, "Multilevel thresholding for image segmentation through an improved quantum-behaved particle swarm algorithm," *IEEE Trans. Instrum. Meas.*, vol. 59, no. 4, pp. 934–946, Apr. 2010.

[2] C. Zhou, L. Tian, H. Zhao, and K. Zhao, "A method of two-dimensional Otsu image threshold segmentation based on improved firefly algorithm," in *Proc. IEEE Int. Conf. Cyber Technol. Autom., Control, Intell. Syst. (CYBER)*, Jun. 2015, pp. 1420–1424.

[3] H. Mittal and M. Saraswat, "An optimum multi-level image thresholding segmentation using non-local means 2D histogram and exponential Kbest gravitational search algorithm," *Eng. Appl. Artif. Intell.*, vol. 71, pp. 226–235, May 2018.

[4] X. L. Zhao and M. Turk, "A multilevel image thresholding segmentation algorithm based on two-dimensional K-L divergence and modified particle swarm optimization," *Appl. Soft Comput.*, vol. 48, pp. 151–159, Nov. 2016.

[5] A. Ben Ishak, "A two-dimensional multilevel thresholding method for image segmentation," *Appl. Soft Comput.*, vol. 52, pp. 306–322, Mar. 2017.

[6] S. Sarkar and S. Das, "Multilevel image thresholding based on 2D histogram and maximum Tsallis entropy—A differential evolution approach," *IEEE Trans. Image Process.*, vol. 22, no. 12, pp. 4788–4797, Dec. 2013.

[7] H. S. N. Alwerfali, M. Abd Elaziz, M. A. A. Al-Qaness, A. A. Abbasi, S. Lu, F. Liu, and L. Li, "A multilevel image thresholding based on hybrid salp swarm algorithm and fuzzy entropy," *IEEE Access*, vol. 7, pp. 181405–181422, 2019.

[8] A. H. del Río, I. Aranguren, D. Oliva, M. A. Elaziz, and E. Cuevas, "Efficient image segmentation through 2D histograms and an improved owl search algorithm," *Int. J. Mach. Learn. Cybern.*, vol. 12, no. 1, pp. 131–150, Jan. 2021.

[9] L. Peng and D. Zhang, "An adaptive Lévy flight firefly algorithm for multilevel image thresholding based on Rényi entropy," *J. Supercomput.*, vol. 78, no. 5, pp. 1–22, 2021.

[10] L. Aranguren, A. Valdivia, M. Pérez-Cisneros, D. Oliva, and V. Osuna-Enciso, "Digital image thresholding by using a lateral inhibition 2D histogram and a mutated electromagnetic field optimization," *Multimedia Tools Appl.*, vol. 81, no. 7, pp. 1–27, 2022.

[11] Q. Deng, Z. Shi, and C. Ou, "Self-adaptive image thresholding within nonextensive entropy and the variance of the gray-level distribution," *Entropy*, vol. 24, no. 3, pp. 319–334, 2022.

[12] M. K. Naik, R. Panda, A. Wunnava, B. Jena, and A. Abraham, "A leader Harris hawks optimization for 2-D Masi entropy-based multilevel image thresholding," *Multimedia Tools Appl.*, vol. 80, nos. 28–29, pp. 35543–35583, Nov. 2021.

[13] B. Lei and J. Fan, "Infrared pedestrian segmentation algorithm based on the two-dimensional Kaniadakis entropy thresholding," *Knowl.-Based Syst.*, vol. 225, pp. 107089–107102, Aug. 2021.

[14] B. Lei and J. Fan, "Adaptive granulation Renyi rough entropy image thresholding method with nested optimization," *Expert Syst. Appl.*, vol. 203, Oct. 2022, Art. no. 117378.

[15] B. Lei, J. Fan, and J. Xu, "An efficient infrared pedestrian segmentation algorithm based on weighted maximum entropy thresholding," in *Proc. Int. Conf. Natural Comput., Fuzzy Syst. Knowl. Discovery*. Cham, Switzerland: Springer, 2021, pp. 1084–1092.

[16] S. J. Mousavirad, D. Oliva, R. K. Chakrabortty, D. Zabihzadeh, and S. Hinojosa, "Population-based self-adaptive generalised Masi entropy for image segmentation: A novel representation," *Knowl.-Based Syst.*, vol. 245, Jun. 2022, Art. no. 108610.

[17] A. Faramarzi, M. Heidarinejad, B. Stephens, and S. Mirjalili, "Equilibrium optimizer: A novel optimization algorithm," *Knowl.-Based Syst.*, vol. 191, Mar. 2020, Art. no. 105190.

[18] H. Karami, M. V. Anaraki, S. Farzin, and S. Mirjalili, "Flow direction algorithm (FDA): A novel optimization approach for solving optimization problems," *Comput. Ind. Eng.*, vol. 156, Jun. 2021, Art. no. 107224.

[19] S. Dhargupta, M. Ghosh, S. Mirjalili, and R. Sarkar, "Selective opposition based grey wolf optimization," *Expert Syst. Appl.*, vol. 151, Aug. 2020, Art. no. 113389.

[20] S. Mahajan, L. Abualigah, A. K. Pandit, and M. Altalhi, "Hybrid Aquila optimizer with arithmetic optimization algorithm for global optimization tasks," *Soft Comput.*, vol. 26, pp. 1–19, May 2022.

[21] P. G. Asteris, A. Mamou, M. Hajihassani, M. Hasanipanah, M. Koopialipoor, T. T. Le, N. Kardani, and D. J. Armaghani, "Soft computing based closed form equations correlating L and N-type Schmidt hammer rebound numbers of rocks," *Transp. Geotechnics*, vol. 29, pp. 100588–100605, Jul. 2021.

[22] N. R. Pal and S. K. Pal, "Some properties of the exponential entropy," *Inf. Sci.*, vol. 66, nos. 1–2, pp. 119–137, Dec. 1992.

[23] D. Martin, C. Fowlkes, D. Tal, and J. Malik, "A database of human segmented natural images and its application to evaluating segmentation algorithms and measuring ecological statistics," in *Proc. 8th IEEE Int. Conf. Comput. Vis. (ICCV)*, Jul. 2001, pp. 416–423.

[24] *Image Segmentation Benchmark Indices Package*. Accessed: Apr. 2, 2022. [Online]. Available: http://www.eecs.berkeley.edu/yang/software/lossy_segmentation/SegmentationBenchmark.zip

RUTUPARNA PANDA (Member, IEEE) was born in 1963. He received the B.Sc.Engg. and M.Sc.Engg. degrees from the UCE Burla, in 1985 and 1988, respectively, and the Ph.D. (Engg.) degree from the IIT, Kharagpur, in 1998.

He was the Former HOD of the ECE Department, the HOD of the CSE Department, the Dean of Academic Affairs, the DEAN of the SRIC, and the Dean of the Continuing Education Program. He is currently a Professor with the Department of Electronics and Telecommunication Engineering, VSS University of Technology, Burla. He has guided 37 M.Tech. theses and eight Ph.D. theses. He has over 180 papers in international/national journals and conferences. He has more than 2000 academic citations with H-index of 26 and i10-index of 49 as per Google scholar. He is the coauthor of two books titled *AI Techniques for Biomedical Engineering Applications* and *Region Based Approaches for Image Fusion: Theories, Techniques and Applications*. He is also the coauthor of eight book chapters. His research interests include digital signal/image processing, bioinformatics, biomedical engineering, VLSI signal processing, soft computing, machine intelligence, and AI. He is a fellow of IETE, India. He received 'Highly Cited Research Award' from *Swarm and Evolutionary Computation* journal (Elsevier), in December 2016. He received the Certificate of Appreciation Award for quality research journal publications for the year 2020 from the VSS University of Technology. His one article is found in top ten popular articles of IEEE Reviews in Biomedical Engineering. He is a reviewer of many reputed international journals like IEEE TRANSACTIONS and Elsevier journals. He serves the editorial board of the *Engineering Applications of Artificial Intelligence* journal indexed by Thomson ISI.

MONORAMA SWAIN (Member, IEEE) was born in 1981. She received the B.E. degree from the Synergy Institute of Engineering and Technology, Dhenkanal (Biju Patanaik University of Technology, Rourkela), the master's degree from the VSSUT, Burla, India, and the Ph.D. degree from the Biju Patanaik University of Technology, in the area of speech emotion recognition. She lead as a PI in a DST sponsored project. She is currently working as a Senior Assistant Professor with the Department of Electronics and Communication Engineering, Silicon Institute of Technology, Bhubaneswar, India. Her research interests include audio digital signal processing, speech processing, image processing, emotion recognition, machine learning, and AI. She is a member of the IEEE Signal Processing and Institution of Engineers. She received the Institution Award from IEI, Odisha, and a Best Teacher Award from ISTE Odisha Section. She served as a Reviewer for *IET Signal Processing* and IEEE Women in Engineering.

MANOJ KUMAR NAIK (Member, IEEE) was born in 1979. He received the master's and Ph.D. degrees from the VSSUT, Burla, India, in 2006 and 2017, respectively. He is currently an Associate Professor at the Faculty of Engineering and Technology, SOA, Bhubaneswar, India. He served more than 16 years in teaching and research. He has guided two M.Tech. theses and two Ph.D. theses. His research interests include soft computing, nature-inspired algorithm, digital signal/image processing, machine intelligence, and AI. In this area, he has contributed 26 papers in international journals and conferences. He is the coauthor of three book chapters. He has more than 400 academic citations with H-index of 10 and i10-index of 11 as per Google scholar. He is a reviewer of many reputed international journals like *Applied Soft Computing* (Elsevier), *Ocean Engineering* (Elsevier), *Biomedical Signal Processing and Control* (Elsevier), and *Engineering Applications of Artificial Intelligence* (Elsevier).

SANJAY AGRAWAL (Member, IEEE) was born in 1972. He received the B.E. and M.Tech. degrees from the UCE Burla, in 1995 and 2003, respectively, and the Ph.D. (Engg.) degree from Sambalpur University, in 2015. He is currently a Professor with the Department of Electronics and Telecommunication Engineering, VSS University of Technology, Burla. He has guided 18 M.Tech. theses and three Ph.D. theses. He has over 50 papers in international journals and conferences. He has more than 1000 academic citations with H-index of 14 and i10-index of 16 as per Google scholar. He is the coauthor of two books and many book chapters. His research interests include digital signal/image processing, bioinformatics, biomedical engineering, soft computing, machine intelligence, and AI.

AJITH ABRAHAM (Senior Member, IEEE) received the Master of Science degree from Nanyang Technological University, Singapore, in 1998, and the Ph.D. degree in computer science from Monash University, Melbourne, VIC, Australia, in 2001. He is currently the Director of Machine Intelligence Research Laboratories (MIR Laboratories), a Not-for-Profit Scientific Network for Innovation and Research Excellence Connecting Industry and Academia. He works as a Professor of artificial intelligence with Innopolis University, Russia, and the Yayasan Tun Ismail Mohamed Ali Professorial Chair of Artificial Intelligence with UCSI, Malaysia. The Network with HQ in Seattle, WA, USA, is also more than 1,500 scientific members from over 105 countries. As an investigator/co-investigator, he has won research grants worth over more than 100 Million U.S. Dollar. He also holds two university professorial appointments. He works in a multi-disciplinary environment and he has authored/coauthored more than 1,400 research publications out of which there are more than 100 books covering various aspects of computer science. One of his books was translated to Japanese and a few other articles were translated to Russian and Chinese. He has more than 46,000 academic citations (H-index of more than 102 as per Google scholar). He has given more than 150 plenary lectures and conference tutorials (in more than 20 countries). He was the Chair of the IEEE Systems Man and Cybernetics Society Technical Committee on Soft Computing (which has over more than 200 members), from 2008 to 2021, and served as a Distinguished Lecturer for the IEEE Computer Society representing Europe, from 2011 to 2013. He was the Editor-in-Chief of *Engineering Applications of Artificial Intelligence* (EAAI), from 2016 to 2021, and serves/served the editorial board of over 15 international journals indexed by Thomson ISI.